Impact of latitudinal variations in vertical diffusivity on climate simulations

M. Jochum[1]

[1]   The currently available theoretical and observational evidence for a latitudinal structure of thermocline vertical diffusivity is synthesized and included in a state of the art coupled climate model. Compared to the standard background value of 0.1 cm^2 s^{-1}, the simulations with the latitudinal structure show only little change in the meridional overturning circulation or northward heat transport. However, two regions are identified which are sensitive to the value of vertical diffusivity: the equatorial band, where only small changes in sea surface temperature lead to precipitation responses with basin-wide teleconnections, and the North Atlantic, where diffusivity affects the spiciness of Labrador Sea water and subsequently the Gulf Stream path.

1.   Introduction

[2]   Most of the world ocean consists of cold water that is formed in high latitudes [*Warren*, 1981]. From this, the relatively warm water of both hemispheres (defined as Warmwassersphäre by *Wüst* [1949]) is separated by the thermocline. The sharpness of the thermocline is highlighted by the success of thermocline theories that treat the abyssal ocean as stagnant and homogeneous [*Luyten et al.*, 1983]. The areas of the ocean surface that are bounded by isotherms of the Warmwassersphäre with $\theta_0 \geq 19°$ have net heat fluxes into the ocean [*Speer and Tziperman*, 1992], and the bounding isotherms are nearly isopycnals, so that air-sea heat flux has to be balanced by diapycnal fluxes across the thermocline [*McWilliams et al.*, 1996]. The mechanical energy required to mix and to lift cold water across the thermocline comes largely from the breaking of internal waves [*Wunsch and Ferrari*, 2004].

[3]   This connection between diapycnal mixing and ocean heat uptake suggests that the ocean poleward heat transport and global climate depends at least partly on the magnitude of mechanical energy available to the generation and dissipation of internal waves. Scaling arguments and ocean general circulation models (OGCMs) support this view [e.g., *Bryan*, 1987; *Scott and Marotzke*, 2002], with the caveat that, by design, the vertical mixing is independent of the surface fluxes and the atmospheric state is independent of the ocean.

[4]   Much then rests on the magnitude and spatial-temporal structure of diapycnal mixing in the thermocline. In principle there are 2 ways to arrive at an estimate: a large-scale balance between surface fluxes and diffusion [e.g., *Walin*, 1982], and direct observations [e.g., *Gregg*,

1977]. However, both approaches are riddled with challenges, many of which are related to the approximations needed to relate fundamental thermodynamics to observables like mean temperature or density microstructure [*Davis*, 1994a, 1994b]. Because of these uncertainties the value of vertical thermocline diffusivity (simply diffusivity from here on) in OGCMs is typically constant in space and time. Earlier OGCMs used a value of 0.3 cm^2/s [*Bryan and Lewis*, 1979], newer vertical mixing schemes like *Large et al.* [1994] now use 0.1 cm^2/s to be consistent with estimates of *Ledwell et al.* [1998]. Fortunately both values generate realistic stratification and northward heat transport in coupled general circulation models (GCMs), and in the absence of more observations it is reasonable to use GCMs with a constant diffusivity to study today's climate. However, to understand future and past climate one has to worry if and how diffusivity can change over time.

[5]   The energy sources for diffusivity are tides and wind, both of which are estimated to contribute similar amounts [*Munk and Wunsch*, 1998]. To have confidence in GCM simulations of past or future climate one needs to understand the connection between these sources and how the energy cascades down to the small scales on which it is eventually dissipated. However, even the magnitude of these energies is difficult to determine, let alone the variations of their sinks (internal wave breaking) in time and space [*Wunsch and Ferrari*, 2004]. Given these difficulties, it is very promising that recent studies report observations of the spatial structure of diffusivity that are consistent with theoretical predictions [*Gregg et al.*, 2003].

[6]   The present study assesses the impact that such a spatially varying diffusivity has on a coupled GCM. The coupled approach is motivated by recent results of *Jochum and Potemra* [2008] which suggest that even minor changes in the thermal structure of the ocean can lead to large tropical precipitation responses. The next section describes the model configuration and the structure of the prescribed diffusivity, section 3 discusses the local results in the forced

---

[1]National Center for Atmospheric Research, Boulder, Colorado, USA.

experiments, and section 4 discusses the global results of the coupled experiments. Section 5 summarizes the results and provides a discussion.

2. Description of Model and Experiment

[7] The numerical experiments are performed using the National Center for Atmospheric Research (NCAR) Community Climate System Model (CCSM) version 3.4 which consists of the fully coupled atmosphere, ocean, land and sea ice models. A detailed description of the released version 3.0 is given by *Collins et al.* [2006]. The main differences between version 3.4 and 3.0 are that the atmospheric general circulation model (AGCM) now uses a finite volume dynamical core [*Bala et al.*, 2008] and an improved convection parameterization [*Neale et al.*, 2008], and that the viscosity in the ocean model is now reduced by 2 orders of magnitude [*Jochum et al.*, 2008].

[8] We use the FV2x1 resolution version of the model in its present-day setup. The ocean model (Parallel Ocean Program, POP) has a horizontal resolution that is constant at $1.125°$ in longitude and varies from $0.27°$ at the equator to approximately $0.7°$ in high latitudes. In the vertical there are 60 depth levels; the uppermost layer has a thickness of 10 m, the deepest layer has a thickness of 250 m. The AGCM uses a horizontal resolution of $1.9° \times 2.5°$ with 26 vertical levels. The sea ice model shares the same horizontal grid as the ocean model and the land model is on the same horizontal grid as the AGCM.

[9] For the present study the most relevant aspect of the model formulation is the vertical mixing parameterization of the ocean model which is a combination of 3 different components: a K profile parameterization for the surface mixed layer [*Large et al.*, 1994], a tidal mixing parameterization for the abyss [*Jayne*, 2008], and constant background diffusivity everywhere else. This constant background diffusivity determines the mixing across the thermocline and is the present focus.

[10] The first global estimate of diffusivity was based on tracer observations and suggested an abyssal value of 1 cm^2 s^{-1} [*Munk*, 1966]. Microstructure measurements by *Gregg* [1977] showed that the diffusivity in the thermocline is smaller than in the abyss which led *Bryan and Lewis* [1979] to use a vertical profile of diffusivity which is constant in time and at each depth, with a minimum value of 0.3 cm^2 s^{-1} in the thermocline and a maximum value of 1.3 $cm^2 s^{-1}$ in the abyss. By releasing tracer in the subtropical Atlantic thermocline *Ledwell et al.* [1993, 1998] measured a thermocline diffusivity of 0.12 ± 0.02 cm^2 s^{-1} after 6 months and 0.17 ± 0.02 cm^2 s^{-1} after 30 months. These values led numerical modelers to reduce the value of thermocline diffusivity from 0.3 to 0.1 cm^2 s^{-1} [e.g., *Large et al.*, 1994]. However, the later observation of 0.17 cm^2 s^{-1} should be more representative as a global background value, and is also supported by 2 more recent studies: North Pacific tritium analyses of *Kelley and Scoy* [1999] find a pycnocline diffusivity of 0.15 ± 0.07 cm^2 s^{-1}, and by using Green's functions to optimize the solution of an OGCM, *Menemenlis et al.* [2005] determine the global background diffusivity to be between 0.15 and 0.17 cm^2 s^{-1}.

[11] Recently, observational evidence has been mounting that diffusivity is varying in space and maybe even in time.

Upper ocean diffusivity is enhanced over the continental slope [e.g., *Moum et al.*, 2002], over the topographic ridges of the Southern Ocean [e.g., *Garabato et al.*, 2004; *Thompson et al.*, 2007], in the subtropical band between $20°$ and $30°$ of latitude [e.g., *Hibiya and Nagasawa*, 2004], in the Indonesian Seas [e.g., *Ffield and Gordon*, 1992], along the path of tropical storms [e.g., *Sriver and Huber*, 2007], and reduced near the equator [*Gregg et al.*, 2003]. The reasons for these variations are not only the spatial distribution of sources and sinks, but also the dependence of internal wave dynamics on latitude. This latitudinal structure of diffusivity is the foundation of the present study, because it is not only observed but also expected from theoretical considerations [e.g., *McComas*, 1977; *Müller et al.*, 1986] and direct simulations of the internal tide [*MacKinnon and Winters*, 2005; *Simmons*, 2008]. Furthermore, by using vertical diffusivity as a control parameter in an OGCM adjoint, *Stammer* [2005] shows that diffusivity should be increased in zonal bands across the subtropics.

[12] Thus, the currently often used constant background (and thermocline) diffusivity of 0.1 cm^2 s^{-1} is replaced with (see also Figure 1) (1) 0.01 cm^2 s^{-1} along the equator where the small or absent Coriolis force limits breaking of internal waves [*Gregg et al.*, 2003]; (2) 0.5 cm^2 s^{-1} at $28.9°$N/S to represent Parametric Subharmonic Instability (PSI) of the M_2 tide [*Tian et al.*, 2006; *Alford et al.*, 2007]; and (3) 0.17 cm^2 s^{-1} everywhere else as global mean background [*Ledwell et al.*, 1998]. Eight experiments were performed, four forced OGCM runs, in which the AGCM has been replaced by observed forcing [*Large and Yeager*, 2008], and four coupled runs. The purpose of the forced experiments is to assess the local impact of the diffusivity changes on the ocean; the working assumption being that the model physics is perfect, and initial temperature and salinity distributions are in balance with the forcing fields. Local changes in the OGCM are then due to changes in vertical diffusivity. Because the spatial variation of diffusivity is confined to the tropics and subtropics, the integration time of the forced experiments should be shorter than the timescale of subtropical-tropical exchange ($20-30$ years [*Harper*, 2000]), but longer than the spin-up time for the equatorial oceans ($10-20$ years [*Liu and Philander*, 1995]). The 2 different timescales are not clearly separated, but one has to make a choice and all the forced experiments are integrated for 20 years. Luckily, the diffusive timescale for the thermocline is less than that, approximately 10 years (for a thickness of 50 m and a diffusivity of 0.1 cm^2 s^{-1}). The analyses are based on the annual mean of year 20.

[13] The control experiment has a constant background diffusivity of 0.1 cm^2 s^{-1} (CONTF), in the second experiment the background diffusivity is increased to 0.17 cm^2 s^{-1} everywhere, except for along the equator where it is reduced to 0.01 cm^2 s^{-1} (Ledwell-Equator-Forced, LEQUAF). The third experiment is identical to LEQUAF, but along $28.9°$N/S the diffusivity is increased to 0.5 cm^2 s^{-1} (LEPSIF). The detailed latitudinal structure of the diffusivity fields is shown in Figure 1, and an overview of the forced experiments is provided in Table 1.

[14] The background diffusivity does not only represent physical processes, but it also ensures numerical stability [*Weaver and Sarachik*, 1990]. Therefore, reducing its minimum value from 0.1 to 0.01 cm^2 s^{-1} could potentially lead

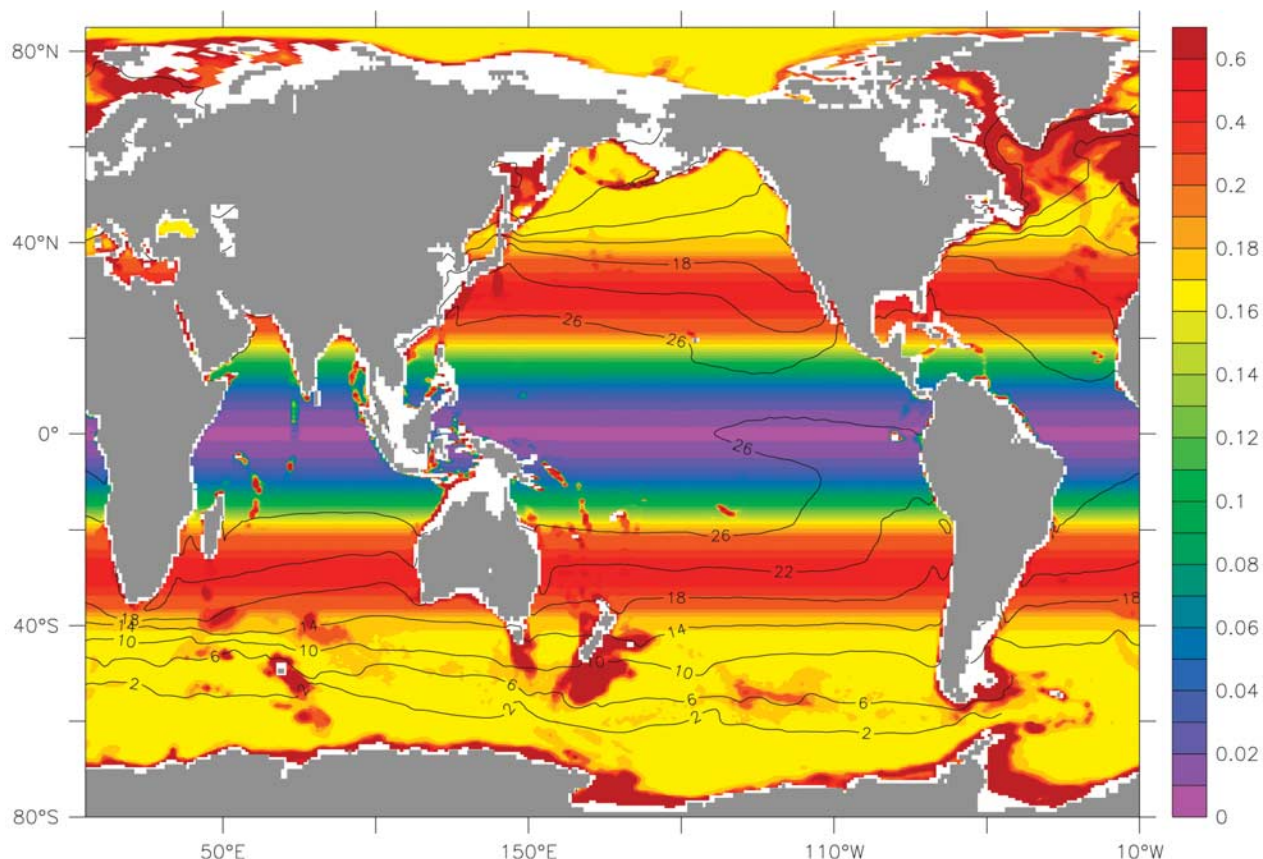**Figure 1.** Vertical diffusivity at 200 m depth. Note the nonequidistant color bar; all values larger than 0.6 cm^2 s^{-1} are in one color and are due to parameterized tidal mixing over shelf and seamounts (based on *Jayne* [2008]). For orientation, the observed SST is superimposed (contour interval 2°C).

to grid-scale noise and numerically induced convection which can lead to a higher effective diffusivity [*Griffies et al.*, 2000]. This is difficult to rule out without checking every timestep of the integration, or repeating the tracer release experiments of *Ledwell et al.* [1993] in the OGCM. Therefore, a fourth experiment is performed in which the equatorial values of LEQUAF are increased by a factor of 3 to 0.03 cm^2 s^{-1} (LEQUA3F). The results for LEQUA3F show that even at these low values the stratification is still sensitive to explicit diffusivity (Figure 2), and one can conclude that the effects of explicit diffusivity still dominate implict, numerically induced diffusivity.

[15] Finally, four coupled experiments were performed, three with OGCM settings identical to forced experiments described above (CONT, LEQUA, and LEPSI), and a fourth which is identical to CONT except for the reduced equatorial diffusivities (EQUA, see Table 1). In all cases, the ocean model is initialized with the January mean climatological potential temperature and salinity (a blending of *Levitus et al.*'s [1998] and *Steele et al.*'s [2001] data sets) and zero velocities. The remaining components are initialized with January conditions obtained from stand-alone integrations. The coupled experiments are integrated for 100 years, and the analysis is based on the means of years 81–100. The length of the coupled runs is determined by the need to

obtain reliable statistics for El Niño/Southern Oscillation (ENSO). Longer runs to assess the changes in the deep ocean are desirable, but very expensive. Given that the differences in abyssal properties during these 100 years are rather small (not shown), the expense could not be justified.

[16] It should be emphasized here again that, although an effort is made to use observed diffusivities, this study does not seek to determine the horizontal structure of thermocline diffusivity. Instead, the purpose is to establish if and where GCMs are sensitive to it, so that future observational, numerical, and theoretical work can be focused on regions

Table 1. List of Experiments and Their Diffusivities[a]

Diffusivities (cm^2 s^{-1})	Global	Equatorial	28.9°N/S
CONTF	0.1	0.1	0.1
LEQUAF	0.17	0.01	0.17
LEPSIF	0.17	0.01	0.5
LEQUA3F	0.17	0.03	0.17
CONT	0.1	0.1	0.1
EQUA	0.1	0.01	0.1
LEQUA	0.17	0.01	0.17
LEPSI	0.17	0.01	0.5

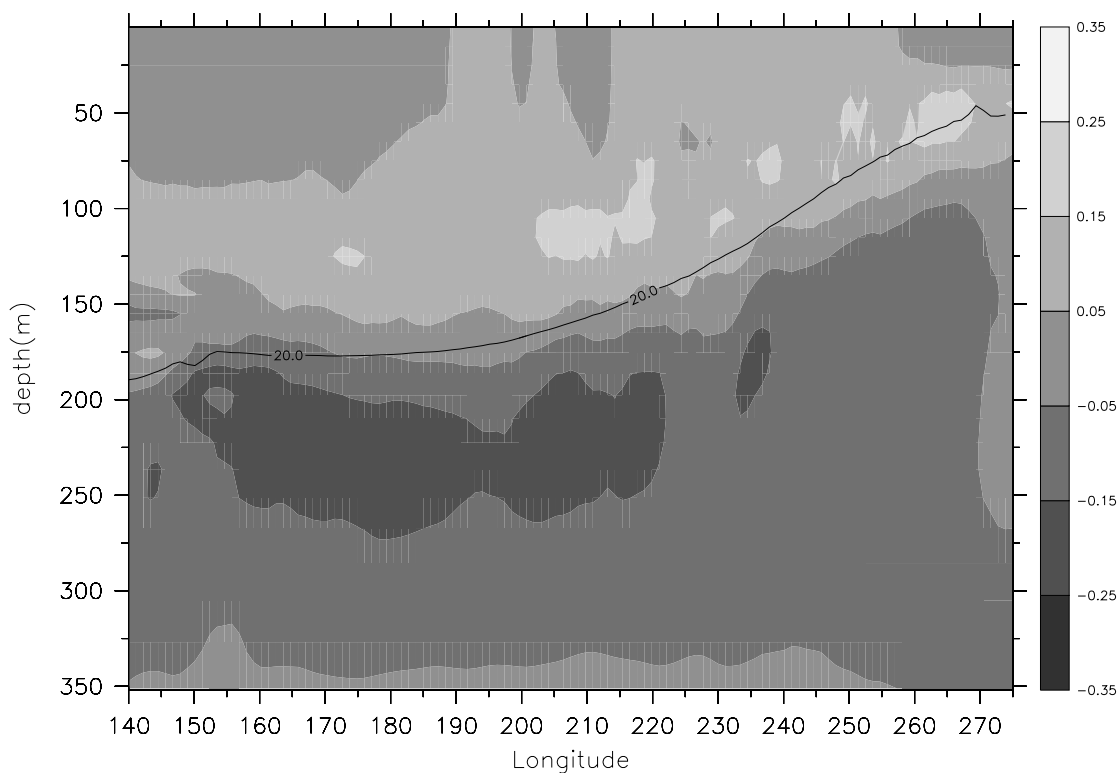[a]The first four experiments are forced OGCM integrations (last letter "F"), the other four are fully coupled integrations.

Figure 2. Temperature difference along the upper equatorial Pacific between a run with $k = 0.01$ cm^2 s^{-1} and a run with $k = 0.03$ cm^2 s^{-1}. Superimposed is the mean position of the 20°C isotherm in LEQUAF. Lower diffusivity reduces diffusion across the thermocline and thereby reduces deeper and increases upper layer temperatures.

where climate is sensitive, rather than regions where mixing is strong.

3. Local Effects in the Forced Simulations

[17] After the sensitivity study of LEQUA3F (Figure 2), the sharpening of the Pacific equatorial thermocline in LEQUAF comes as no surprise (Figure 3, the pattern is similar in the Atlantic and Indian oceans). It is noteworthy, though, that the changes extend far below the thermocline (approximated by the 20°C isotherm). Comparison with TAO data (Figure 4) shows that compared to CONTF the equatorial thermocline improved only marginally. The two largest problems appear to be that the model has been initialized with a too weak thermocline (see results of year 1), and that the depth of maximum stratification (identical to the depth of the core of the Equatorial Undercurrent, EUC) is too deep. The former can be helped with a better initialization procedure, the latter is a common OGCM bias [*Maes et al.*, 1997; *Jochum et al.*, 2008], and both are beyond the scope of the present discussion. It should be pointed out, though, that LEQUAF is able to maintain its original maximum stratification, whereas in CONTF the stratification continues to deteriorate after the initialization. This suggests that once the EUC and the initialization biases are removed, LEQUAF will lead to a more realistic equatorial thermocline.

[18] A section across 110°W reveals that subthermocline cooling in LEQUAF is mostly limited to the region of reduced diffusivity (19°S–19°N, Figure 5), which is similar to the structure and magnitude of the cooling in an tropical Pacific study that uses hybrid vertical coordinates and the same equatorial diffusivity [*Harrison and Hallberg*, 2008]. Although the subthermocline temperatures are reduced by more than 1°C, the velocities of the zonal currents are not changed by much, and the maximum of total upwelling between 5°S and 5°N is reduced in CONTF by only 1 Sv to 67 Sv in LEQUAF. The largest change is in the core of the EUC which increased from 93 cm/s in CONTF to 103 cm/s in LEQUAF, both of which are in reasonable agreement with the observed 97 cm/s [*Johnson et al.*, 2001]. The subthermocline cooling is relevant because in LEQUAF the Tsuchiya Jets at 5°N/S deliver the observed 12°C water to the American upwelling regions [*McCreary et al.*, 2002] rather than the 13°C water in CONTF. This reduces warm biases in coastal sea surface temperature (SST) [*Large and Danabasoglu*, 2006] here and in the coupled model. Because of the strong constraint of the surface boundary conditions in the forced runs, SST will be discussed in detail for the coupled simulations only.

[19] The enhanced diffusivity at 28.9°N/S (LEPSIF) has an effect in contrast to, but consistent with, the results of LEQUAF: cooling above the thermocline and warming below it (Figure 6). Note that as far as the subtropical thermocline is concerned warming/cooling is always associated with saltening/freshening (not shown), because warm and salty water is overlying cold and fresh water formed at higher latitudes. The subthermocline warming happens at all
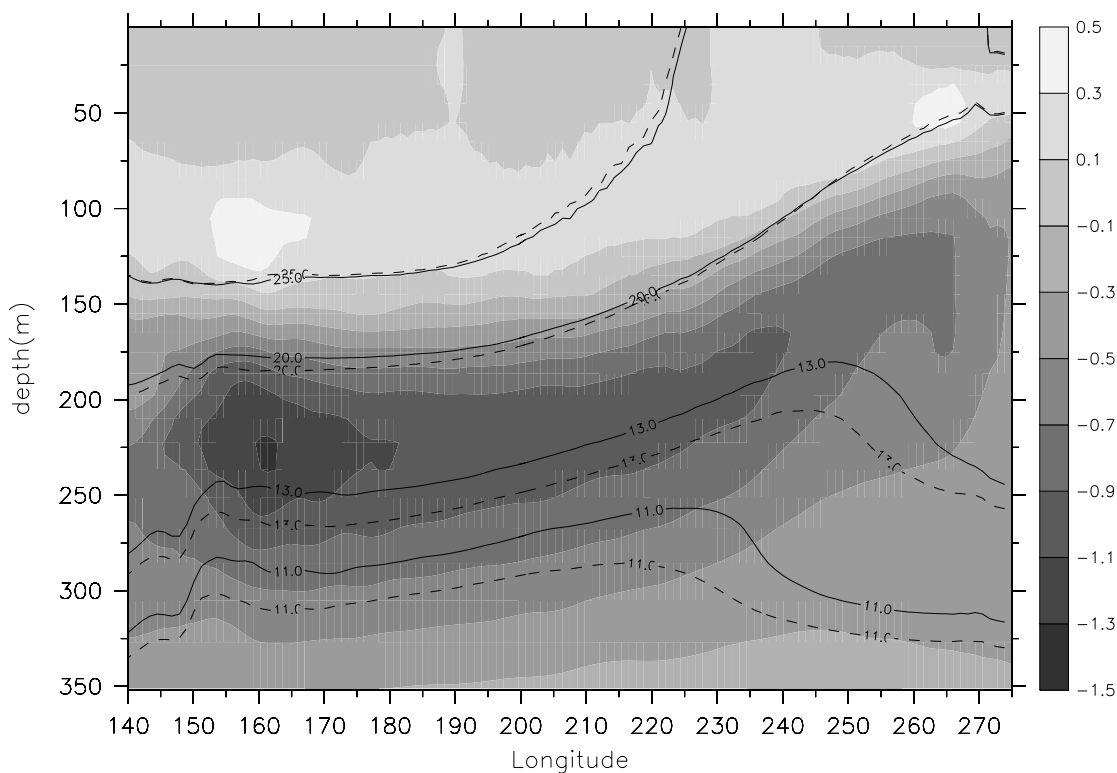
Figure 3. Temperature difference (shades in 0.4°C intervals) between LEQUAF and CONTF along the equator. Superimposed are selected mean isotherms (LEQUAF is shown by the solid lines; CONTF is shown by the dashed lines).

longitudes; the maximum signal is seen at 28.9°N/S and spreads equatorward, consistent with theories and observations of the subtropical cell [*Fine*, 1987; *McCreary and Lu*, 1994]. Note that the equatorial subthermocline cooling in LEQUAF is replaced by a warming as the subtropical water is advected toward the equator (Figure 6). Other than that, the author is not aware that the changes in LEPSIF project significantly on any model biases. For example, the subtropical cooling at 200 m depth in the northern Pacific reduces a model warm bias there, whereas it increases the cold bias in the southern hemisphere. This ambivalence is different from LEQUAF, where the reduced diffusivity at the equator leads to a sharper, more realistic equatorial thermocline in all three basins.

[20] One can speculate that this ambivalence in the bias improvements is reflective of the fundamental asymmetries in the assumptions that are behind LEQUAF and LEPSIF. LEQUAF is based on theories that breaking of internal waves is inhibited along the equator, independent of the available wave energy. Thus, diffusivity should be small everywhere along the equator. PSI, on the other hand, provides only a weak constraint on diffusivity. For the same internal wave field and stratification the diffusivity will be maximal along 28.9°N/S, but in a spatially inhomogeneous wave field the available energy can vary, so that the diffusivity at other latitudes can be larger than at 28.9°N/S if more energy for mixing is available. In fact, *Hibiya and Nagasawa* [2004] find that elevated mixing values do indeed occur equatorward of 30° latitude, but only near and above rough topography. However, the complete three-

or four-dimensional description of diffusivity is still far from complete and is beyond the scope of the present work.

[21] According to the literature discussed in the introduction, diffusivity limits the oceanic uptake of heat. And indeed, we find that compared to CONTF the uptake within the annual mean position of the 19°C isotherm in LEQUAF is slightly reduced from 1.27 to 1.22 precipitable water (PW), and the uptake in LEPSIF is increased to 1.36 PW. Compared to the observed value of 1.57 PW [*Large and Yeager*, 2008], the value in LEPSIF represents an improvement, although it should be kept in mind that heat flux observations are notoriously difficult and uncertain.

4. Global Effects in the Coupled Simulations

[22] The main purpose of the forced simulations in the previous section is to aid the interpretation in the coupled experiments. Because of the long integration time and the atmospheric coupling it is not possible anymore to attribute cause and effect unequivocally. However, with the present set of 8 experiments some insight can still be gained. A first glimpse at the differences in SST (Figure 7) and precipitation (Figure 8) suggests that the present changes to the diffusivity do only lead to modest changes in climate.

[23] However, the following three different changes can be singled out in which there is a coherent structure and whose dynamics and feedbacks deserve discussing (arguably a subjective choice): (1) The shift of equatorial rainfall, most pronounced in the Indian and Pacific oceans, but also visible in the Atlantic (for EQUA only, Figure 8a). (2) The southward shift of the Gulf Stream as manifested by the
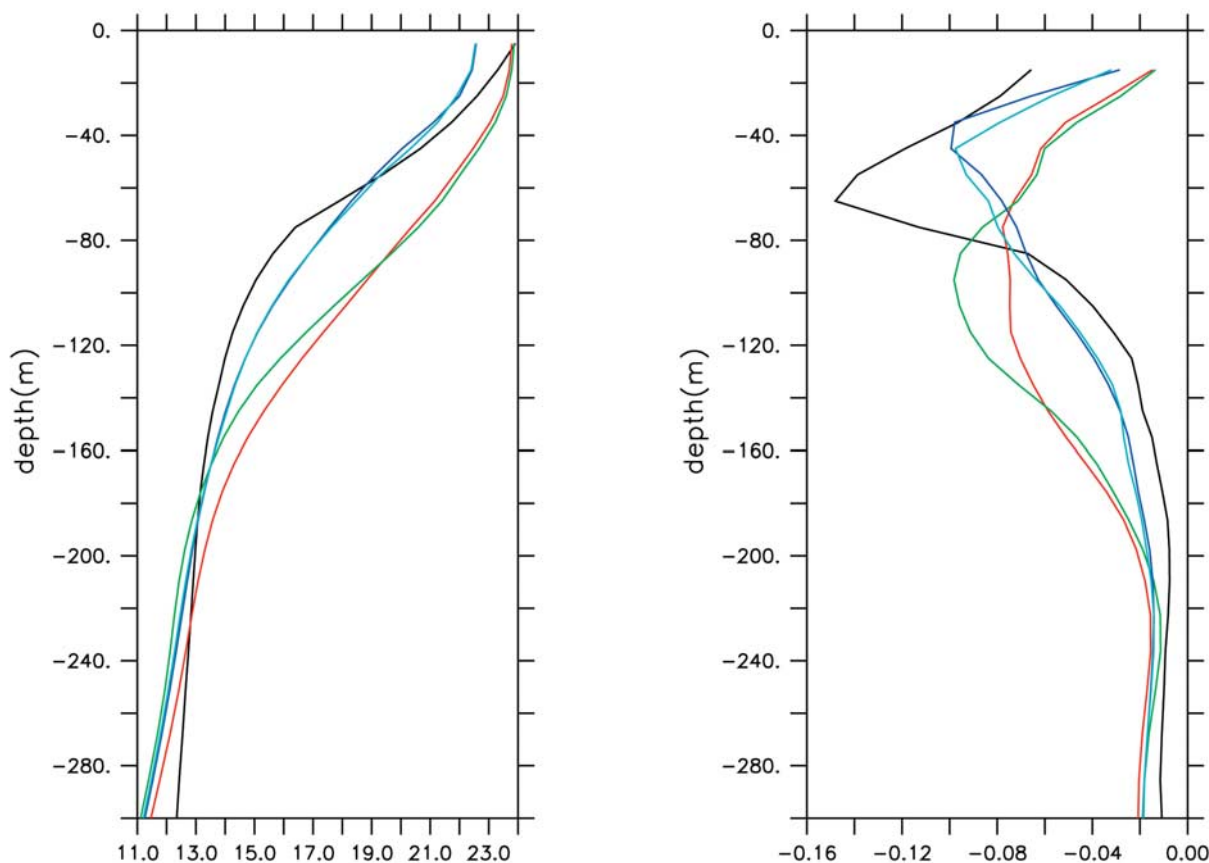
Figure 4. (left) Temperature and (right) temperature gradient profiles at 110°W/0°N for the observations (black lines), CONTF and LEQUAF mean over the first year (light and dark blue lines, respectively) and mean over year 20 (red and green lines, respectively).

large cooling signal in LEQUA and LEPSI (Figures 7b and 7c). (3) The warming of the Labrador Sea (LEQUA and LEPSI, Figures 7b and 7c). Surprisingly, neither the strength of the Atlantic Merdional Overturning Circulation (MOC) nor the northward heat transport change much (Table 2). The change in total heat uptake across the 19°C, too, is small and is consistent with expectations from the forced simulations: little change between CONT and LEQUA, and an approximately 10% increased by adding the increased diffusion along 28.9°N/S (Table 2).

[24] Table 2 also indicates that ENSO activity becomes stronger when diffusivity is reduced along the equator or increased along 28.9°N/S. In all four experiments ENSO has the same spectral characteristics, which are also the same as in CCSM3.4 [see *Neale et al.*, 2008]: a broad peak of energy between 3 and 5 years, with the strongest amplitude in January. While these authors were able to explain the seasonality and the irregularity of ENSO as the result of westerly windburst activity, the processes that determine the amplitude of ENSO are still under investigation. It should be noted, though, that the sharpening of the equatorial thermocline that is apparent in the forced simulations and still present in EQUA is not present anymore in LEPSI. Thus, ENSO strength is not related to thermocline structure alone. A more detailed investigation of ENSO

strength is beyond the scope of the present study. Instead, there follows a discussion of the mean surface signals highlighted under 1–3.

4.1. Equatorial Precipitation

[25] The tropical response is dominated by the reduction of equatorial diffusivity (Figures 7 and 8), so for the sake of simplicity the focus here is on EQUA. From the discussion of the forced results one can expect a general warming of the equatorial sea surface, but the strong tropical air-sea interactions create remote effects that deserve discussion. It is helpful to look at the directly forced response first (EQUAF-CONTF; Figure 9): in response to reduced diffusivity the near-equatorial band warms up, in particular around upwelling regions like the eastern equatorial Pacific, the Costa Rica dome and the southwest Indian Ocean. The cooling seen off the western coasts of North and South America are the results of cooler equatorial subthermocline water advected poleward in the subsurface countercurrents and coastal undercurrents (see previous section).

[26] In the coupled simulation (EQUA) the pattern of surface warming is similar, but leads to shifts in precipitation with subsequent feedbacks. This is most obvious in an arc of cooling that reaches from the northern Pacific along the Californian coast into the west Pacific warm pool (Figure 10). Another, but weaker, shift can be seen in the
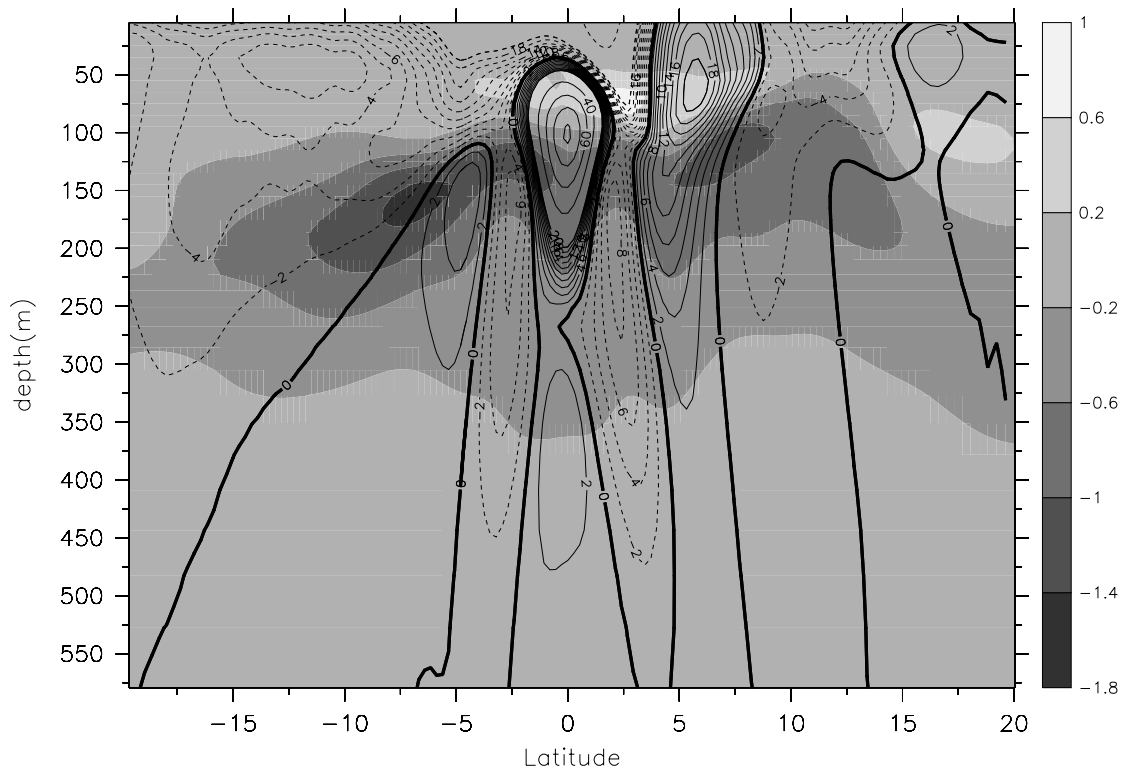
Figure 5.   Temperature difference (shades in 0.4°C intervals) between LEQUAF and CONTF and mean zonal velocity in CONTF (contour lines are 20 cm/s for velocities greater than 20 cm/s and 2 cm/s for smaller velocities) along 110°W.
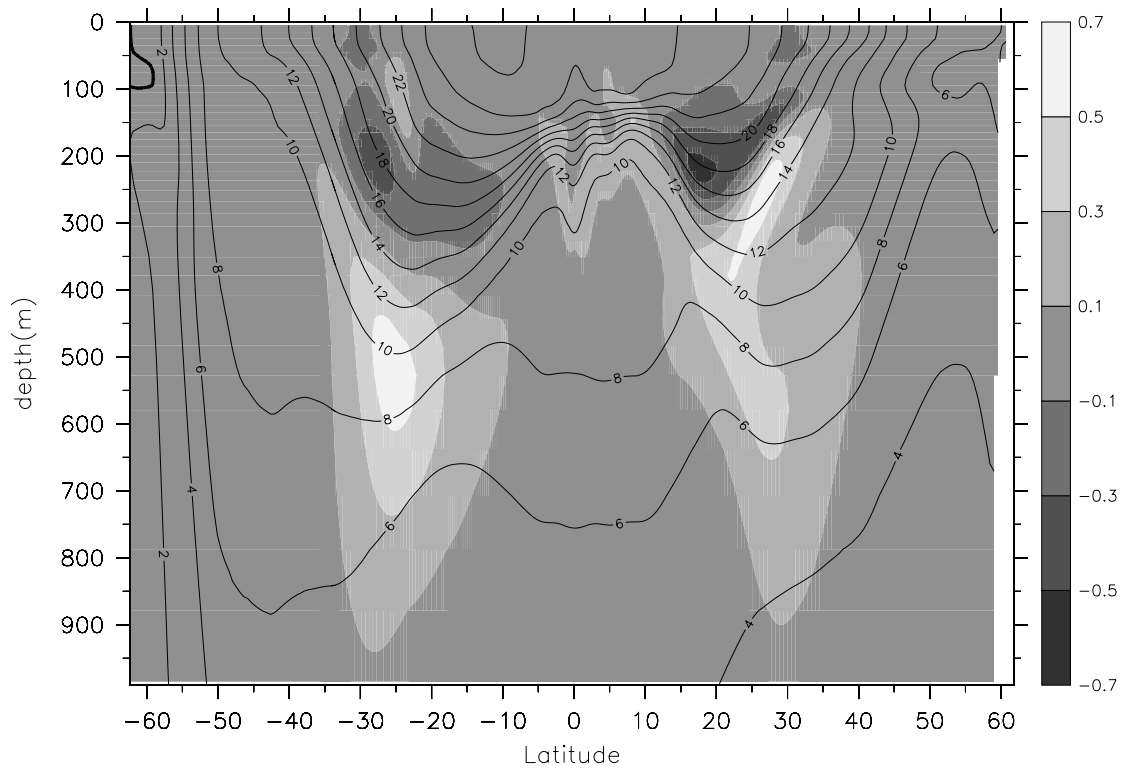

Figure 6.   Temperature difference (shades in 0.2°C intervals) between LEPSIF and LEQUAF and mean temperature in LEQUAF along 150°W.
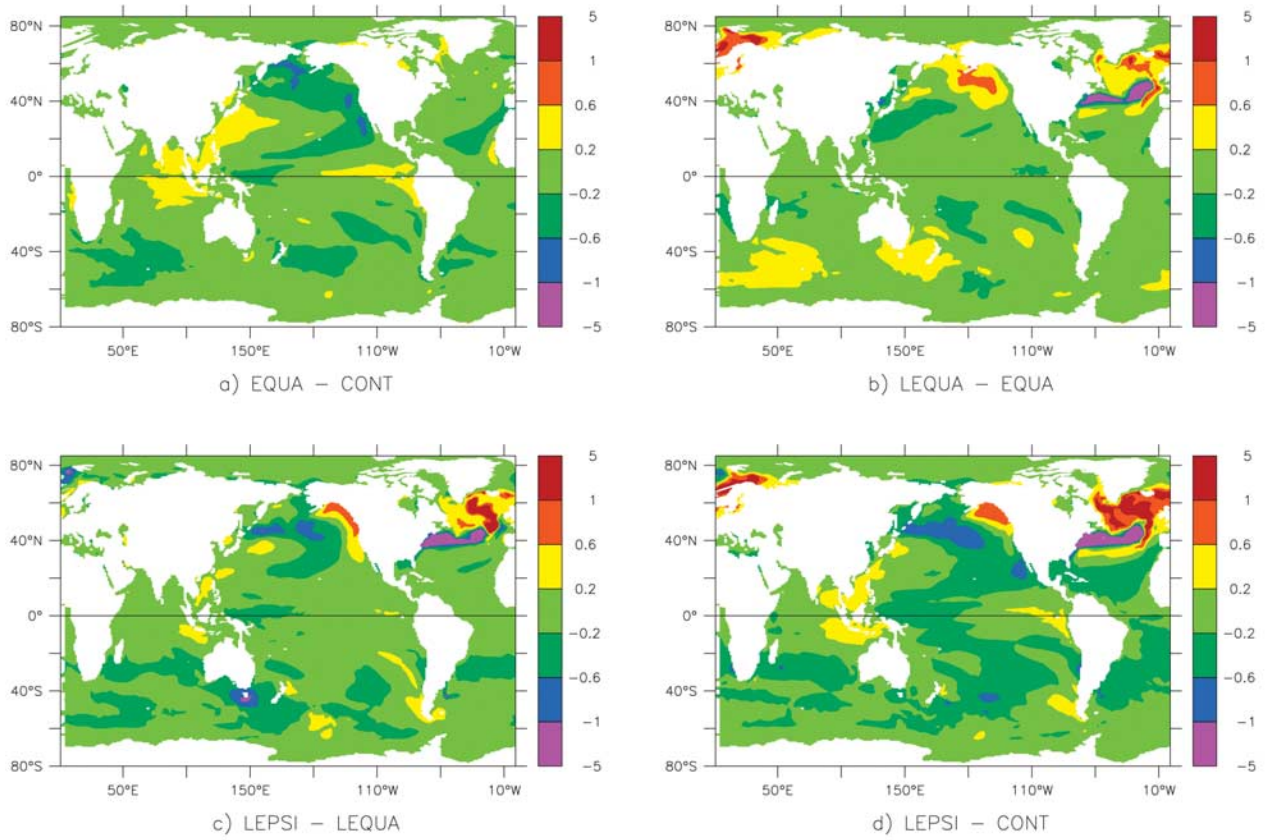
Figure 7. Difference in sea surface temperature between the different experiments.
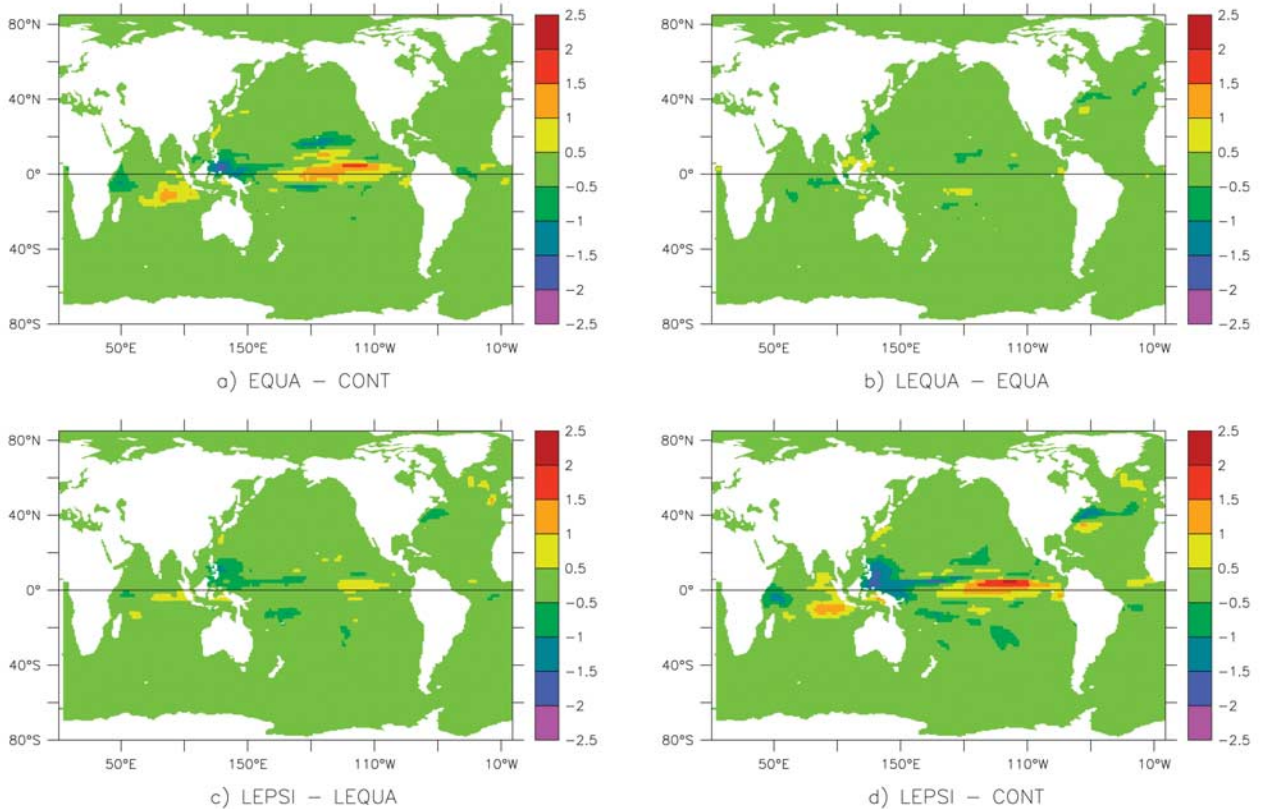

Figure 8. Difference in precipitation between the different experiments (in mm/d).

Table 2. Strength of the Atlantic MOC at the Equator, Maximum Atlantic Northward Heat Transport, Net Heat Uptake Within the 19°C Isotherm, Average Ocean Heat Loss, and the Standard Deviation of the Anomalous NINO3 SST[a]

	MOC (Sv)	Northward (PW)	Downward (PW)	Cooling (W/m²)	NINO3
CONT	17.8	1.13	1.39	0.16	1.1
EQUA	18.1	1.12	1.30	0.32	1.4
LEQUA	18.4	1.12	1.42	0.14	1.4
LEPSI	18.4	1.11	1.52	0.01	1.6

[a]NINO3 SST at 150-90°W and 5°S-5°N

southern Indian ocean where the maximum SST response shifts eastward toward Sumatra and Java. The former response is a well studied atmospheric teleconnection to eastern equatorial Pacific warming (like El Niño), which leads to a strengthening of the subtropical high (Figure 11) and Aleutian Low (not shown [*Livezey et al.*, 1997; *Trenberth et al.*, 1998]). The stronger pressure gradients lead to stronger westerlies and Trade winds, which cool the underlying water in the central tropics and increase the northward heat transport along the western boundary (Figure 10). It is interesting to note that the eastern to central equatorial rain, SST and wind responses are consistent with the results of a recent diffusivity study in a regional high-resolution coupled model (K. Richards et al.,

Vertical mixing in the ocean and its impact on the coupled ocean/atmosphere system in the eastern tropical Pacific, submitted to *Journal of Physical Oceanography*, 2008). The main difference with the present study is the coastal amplification of the changes, which is absent here. It can be speculated that this is due to the generally poor performance of CCSM in coastal upwelling regions [*Large and Danabasoglu*, 2006].

[27] The response in the southern Indian ocean is a direct response to the off equatorial warming which weakens the subtropical high there [*Gill*, 1980], increases precipitation (Figure 10) and weakens the southeasterly Trades (Figure 11). The fact that the maximum SST response is shifted eastward (compared to the forced response) is directly related to the weaker Trades. Especially during boreal summer the monsoon winds along the Sumatra and Java coasts are upwelling favorable [*Schott and McCreary*, 2001], and the reduced strength of the southern Indian ocean subtropical high weakens this coastal upwelling which leads to increased SST.

4.2. North Atlantic, Labrador Sea, and Arctic Ocean

[28] The changes in the Labrador Sea and the Gulf Stream are connected, and both caused by the warming (Figure 6) and saltening (not shown) of the subthermocline subtropical Atlantic. In both the forced and the coupled simulations this subtropical water feeds the Gulf Stream and ultimately
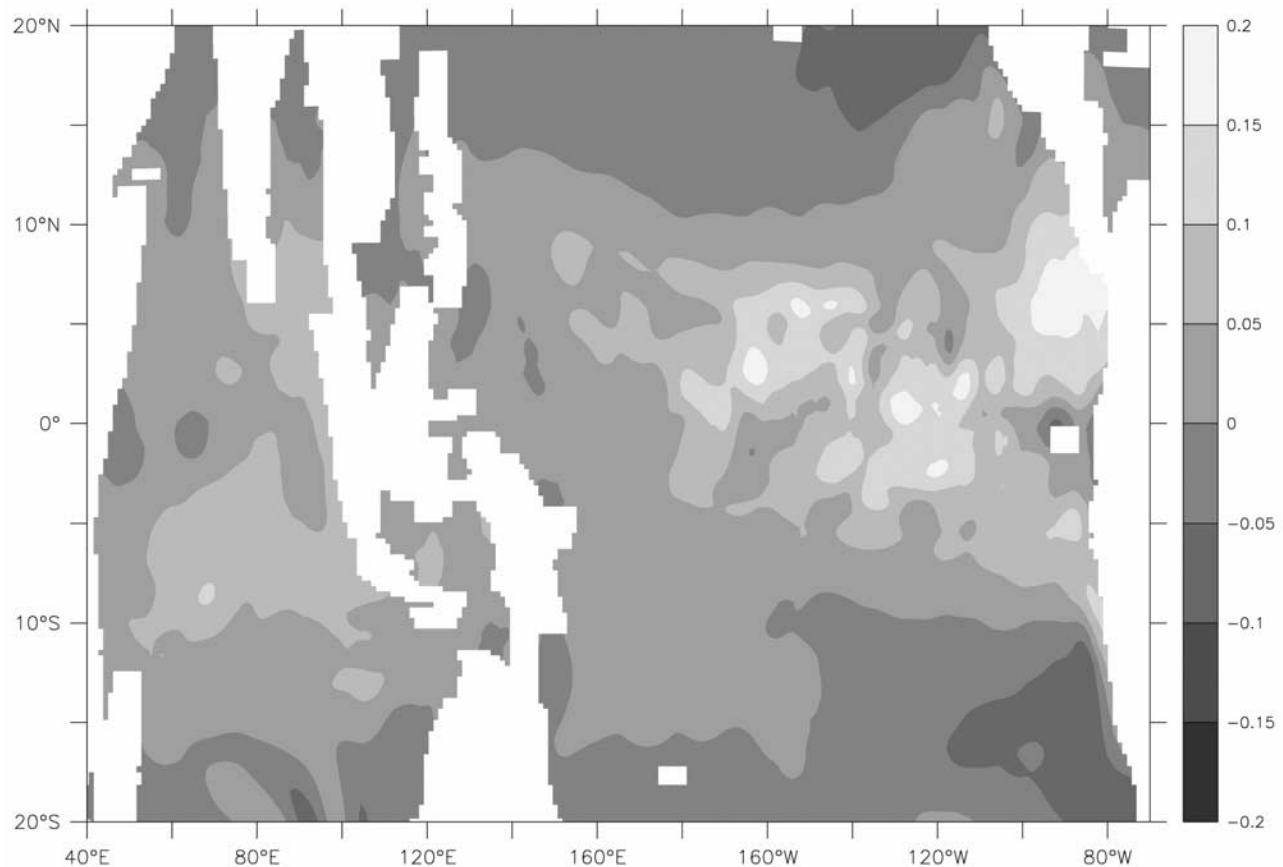

Figure 9. Difference in SST between LEQUAF and CONTF. Note that the differences could be muted because of the upper boundary condition which forces the SST toward the observed air temperature.
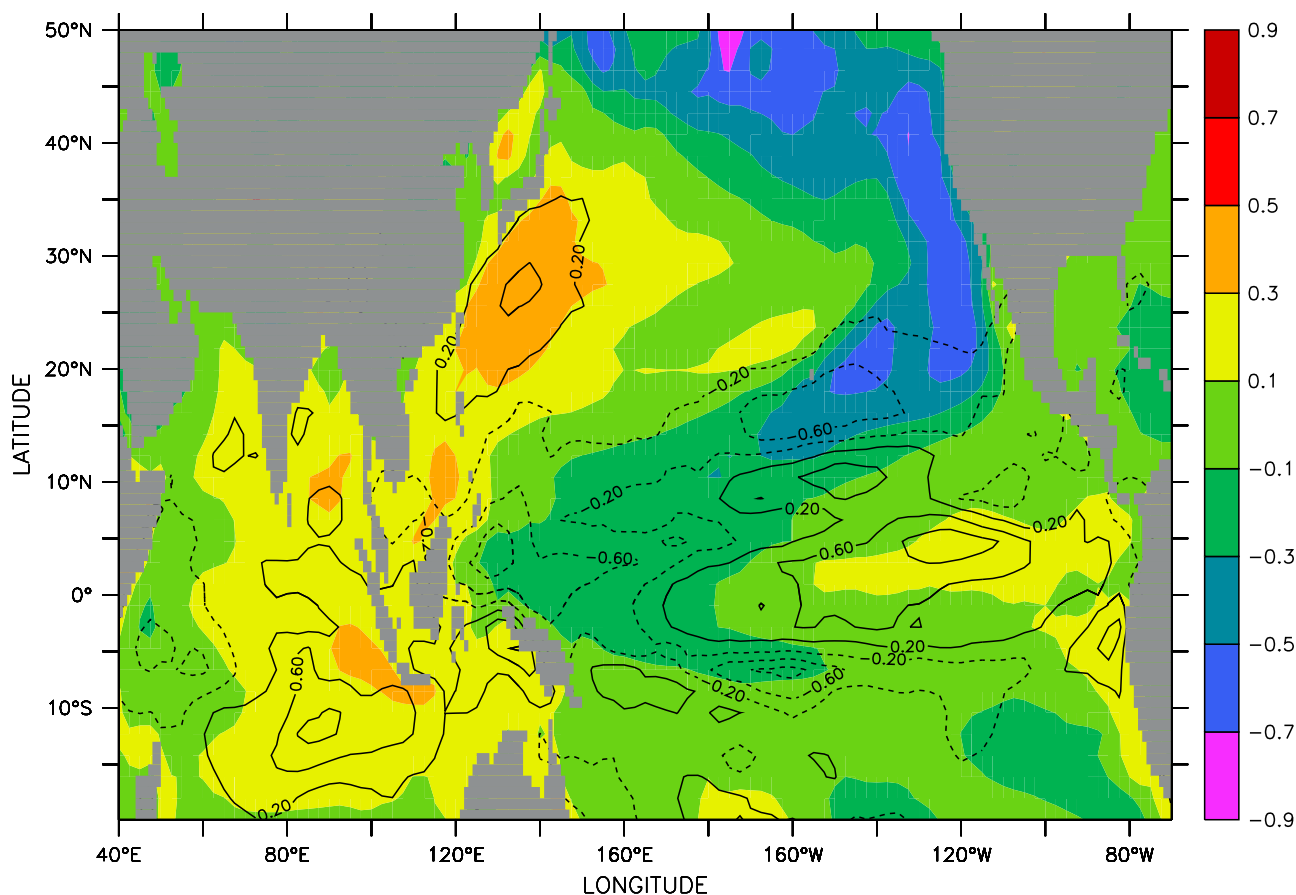
Figure 10. Difference in SST (color) and precipitation (contour lines are 0.4 mm/d) between EQUA and CONT.

supplies the convection regions in Labrador Sea and Arctic oceans (Figure 12). For the sake of argument, it is assumed that both, LEQUA and LEPSI, have a similar effect on the North Atlantic in that they make the Gulf Stream warmer and saltier (Figure 13) and displace it southward (Figures 7b and 7c). These changes to the Gulf Stream water are largely density neutral (not shown), and are advected to the Arctic ocean and Labrador Sea in the North Atlantic drift (Figure 13). The connection between increased subtropical diffusivity and a warmer and saltier subthermocline Gulf Stream and Labrador Sea is described here as solely because of oceanic processes. It is not possible here to rule out conclusively an effect of atmospheric feedback, but the fact that the forced simulations show a similar response (not shown) and that the westerlies are only marginally different between CONT and LEPSI (not shown) supports this view.

[29] The warmer and saltier Labrador Sea is more susceptible to convection (Figure 14), something not obvious and explored in detail by *Bailey et al.* [2005]: Convection is triggered by buoyancy loss, and all things being equal, a larger buoyancy loss will lead to stronger convection and deep water production. For identical densities (the salinity and temperature differences between CONT and LEPSI lead to only small density differences), the same atmospheric conditions will lead to a stronger buoyancy loss for the warmer water, because at these latitudes the atmosphere removes heat more efficiently than freshwater. Moreover,

the warmer Labrador Sea in LEPSI also has a slightly smaller sea-ice cover (not shown). It is beyond the scope of the present manuscript to explore the relative importance of modes of buoyancy loss and difference in sea-ice cover, but the chain of events so far suggests that increased diapycnal diffusivity in the subtropical Atlantic will increase Labrador Sea water production.

[30] Labrador Sea water forms the upper part of the Deep Western Boundary Current (DWBC), the strength and vertical structure of which is one of the factors that determines the separation latitude of the Gulf Stream [*Thompson and Schmitz*, 1989; *Ezer and Mellor*, 1992]. There exists a vast literature to explain this connection which is summarized by *Zhang and Vallis* [2007]. On the basis of their own theoretical and numerical analysis, they conclude that the downslope flow of the DWBC leads to vortex stretching which creates a recirculation gyre south of the Grand Banks. The strength of this recirculation is one of the key processes that determines the separation latitude of the Gulf Stream. Thus, a stronger DWBC leads to a more southerly separation latitude which is consistent with the present results (Figure 15) and the results of *Gerdes and Koeberle* [1995].

[31] It should be pointed out that representation of water mass structure and circulation in the North Atlantic did not improve. Because of the Mediterranean outflow the water mass properties in the subthermocline are sensitive to the
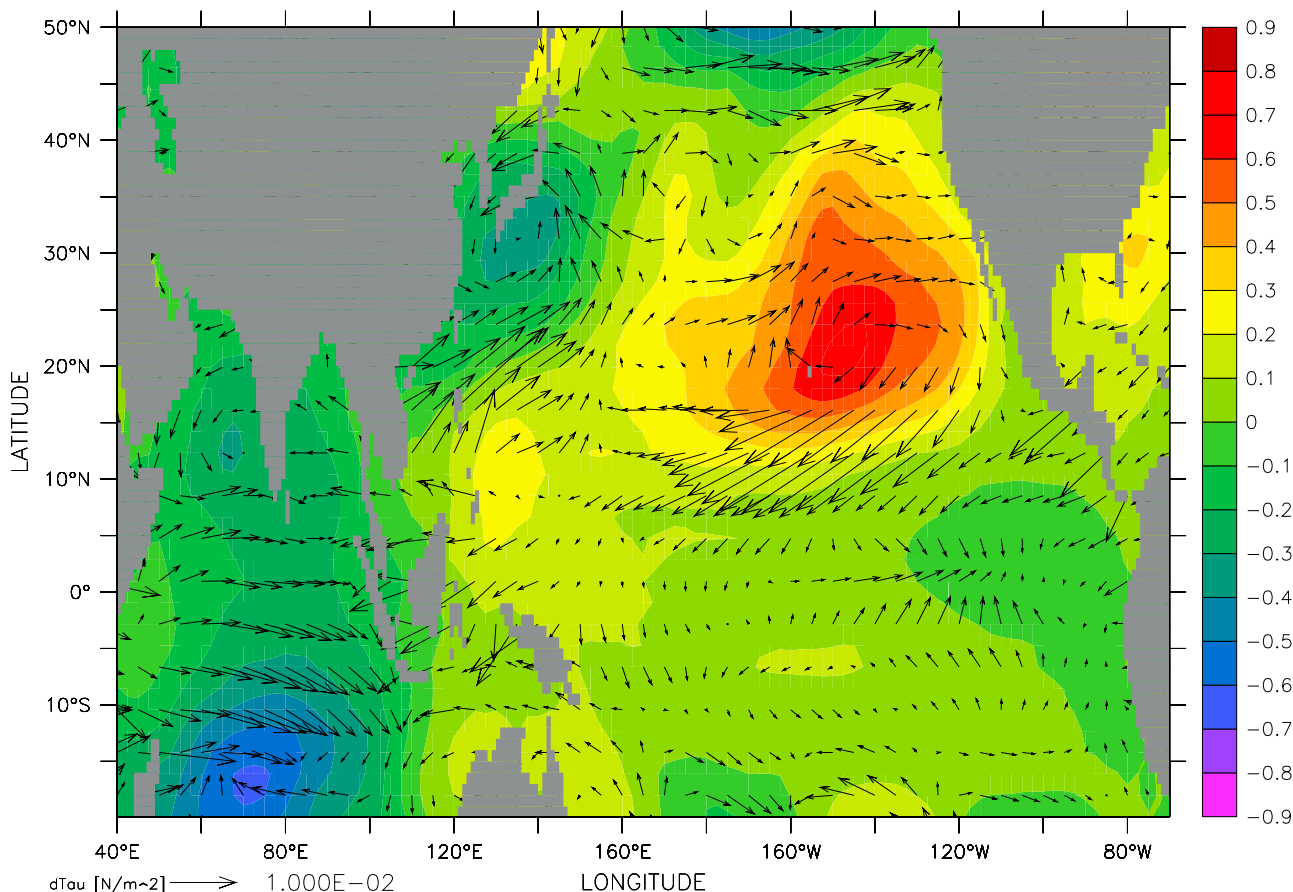
Figure 11. Difference in sea level pressure (color bar, in mbar) and surface wind stress between EQUA and CONT.

Mediterranean freshwater budget, which is not well reproduced in CONT. Thus, the subthermocline North Atlantic is already too warm and salty in CONT, and this bias intensifies in LEPSI. Also, the Gulf Stream separation is a longstanding problem of OGCMs, it is poorly represented in CONT and is worse in LEPSI. However, the increased production of Labrador Sea water and its spreading along the coast is an improvement which may lead to an improved carbon cycle [*Gent et al.*, 2006].

5. Summary and Discussion

[32] An attempt is made to distill the available theoretical, numerical and observational evidence of thermocline vertical diffusivity into a latitudinal profile. Of course, diffusivity varies in time and longitude as well, but for the latitudinal structure there exists some theoretical guidance because breaking of internal waves depends on the local inertial frequency (see section 2).

[33] Current OGCMs, including the present one, typically use a diffusivity of 0.1 cm^2 s^{-1} which is based on the first observations of released tracers in the subtropical North Atlantic. Newer evidence, from other basins as well, suggests that a global mean value should be larger, around 0.17 cm^2 s^{-1}. Theory and observations also suggest that there are latitudinal bands with distinctly different diffusivities: the equator where the diffusivity is reduced, and

28.9°N/S where the diffusivity is increased. While the general increase or decrease in diffusivity can be argued from theory, the magnitude of the change has to be based on observations. The available observations discussed in section 2 suggest a value of 0.01 cm^2 s^{-1} along the equator and a value of 0.5 cm^2 s^{-1} along 28.9° N/S. If we accept this general structure, the question then arises where exactly is diffusivity important enough to justify the expensive experiments that measure it?

[34] With the caveat of the relatively short integration time, the present results suggest that the MOC and the northward heat transport show only a weak sensitivity to the range of diffusivities discussed here. However, two regions are identified which are sensitive to the value of vertical diffusivity: the equatorial band, where only small changes in sea surface temperature lead to precipitation responses with basin-wide teleconnections; and the North Atlantic where diffusivity affects the salinity/temperature ratio of Labrador Sea water and subsequently the Gulf Stream path. Furthermore, the strength of ENSO appears to be sensitive not only to equatorial but also to midlatitude diffusivities, for reasons that are not understood yet.

[35] It cannot be argued that the presented structure of diffusivites leads to significantly improved water mass properties or climate in CCSM. Tropical precipitation does improve, but only minorly so compared to the current biases [see *Large and Danabasoglu*, 2006]. The Gulf Stream
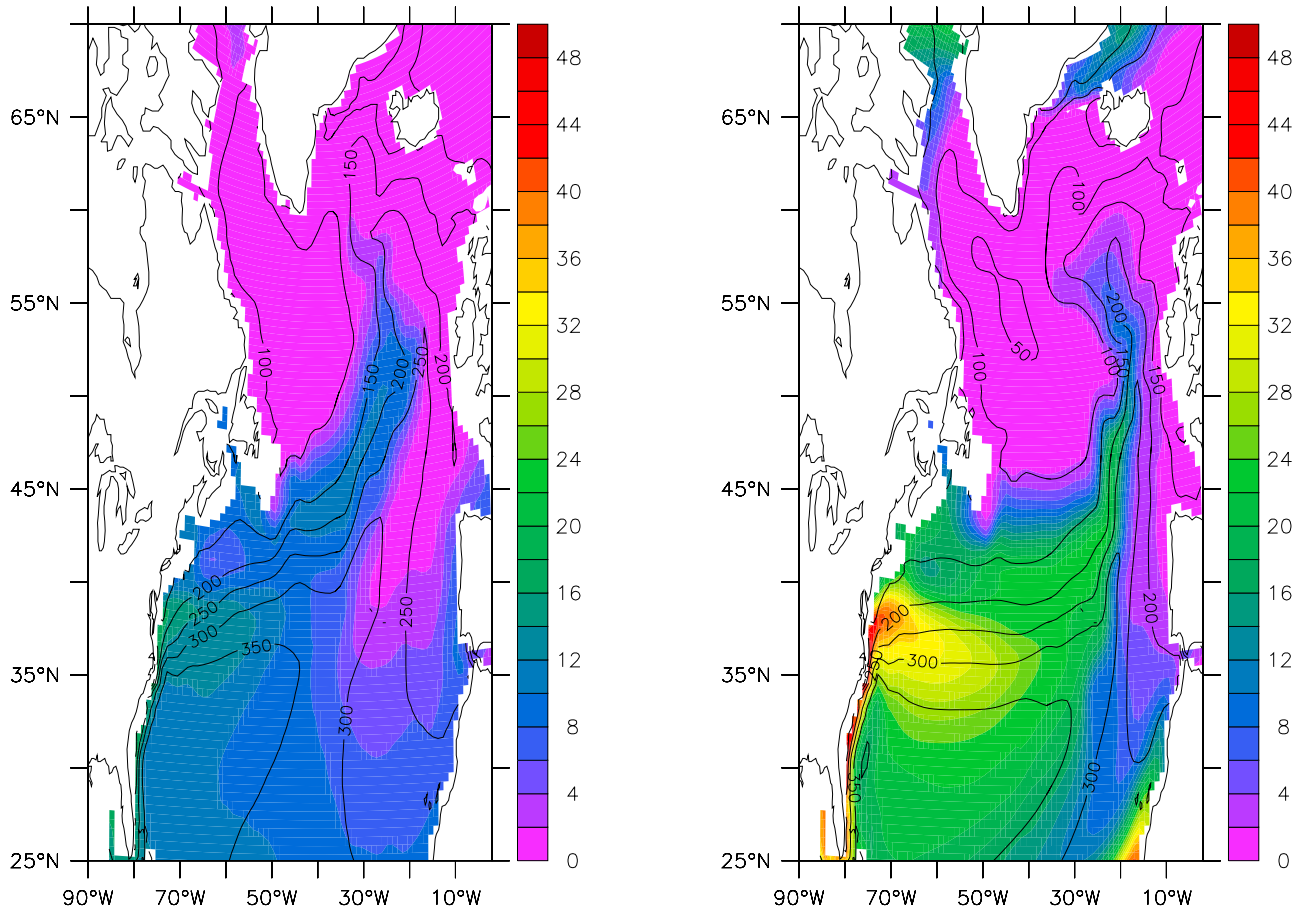
Figure 12. Ideal age tracer on the $\sigma 28$ isopycnal (color bar) and depth of the $\sigma 28$ isopycnal (contour interval is 50 m) for (left) LEPSIF and (right) LEPSI. Note the difference in the integration lengths of the forced (20 years) and coupled (100 years) simulation. The freshly subducted and convected waters are young, whereas the subtropical waters that supply the Gulf Stream are relatively old. The age signal of these old subtropical waters slowly vanishes as the North Atlantic Current entrains younger surrounding waters.
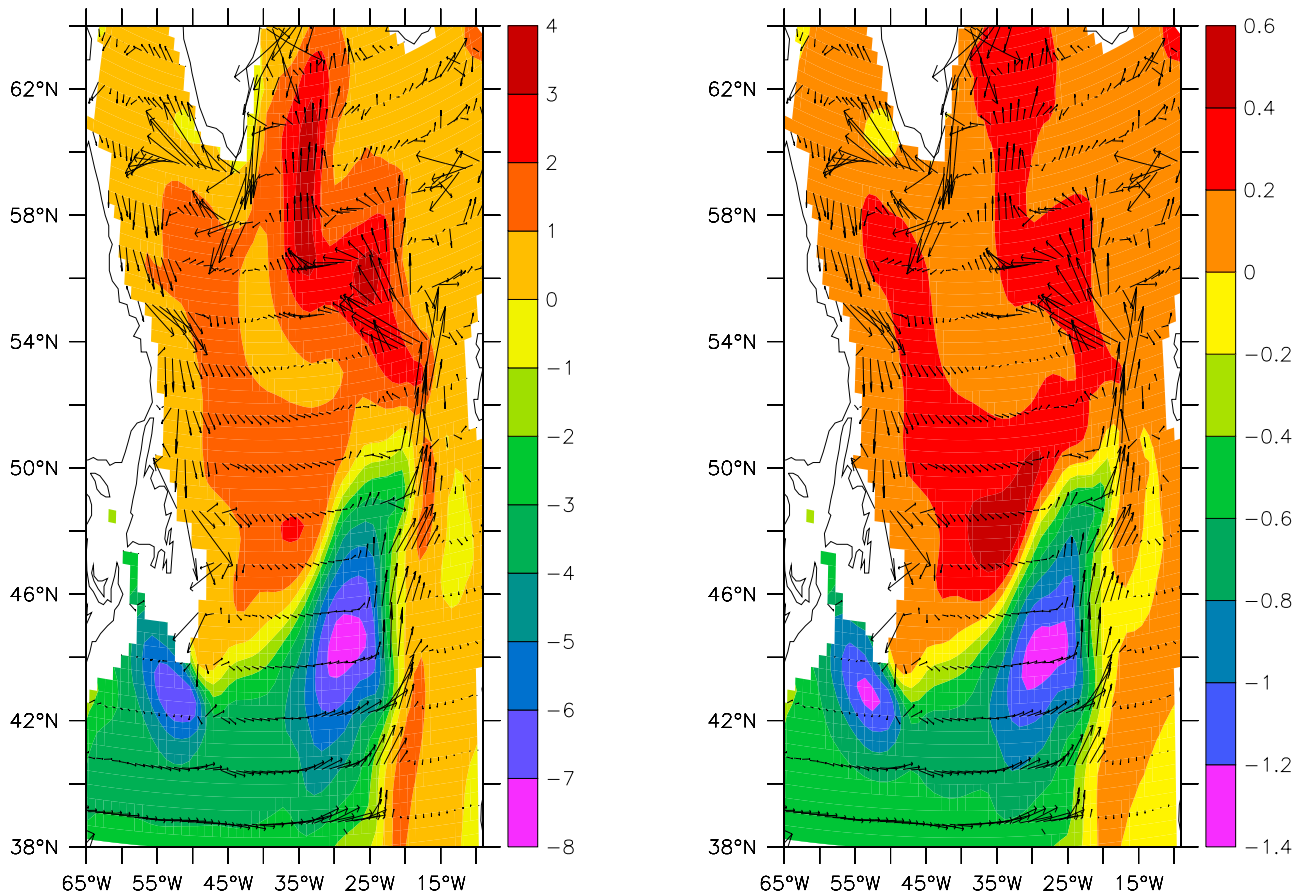
Figure 13. Difference in (left) temperature and (right) salinity on the $\sigma 28$ isopycnal between LEPSI and CONT and velocity (maximum velocities between 30 and 35 cm/s around Greenland) on this surface in LEPSI.
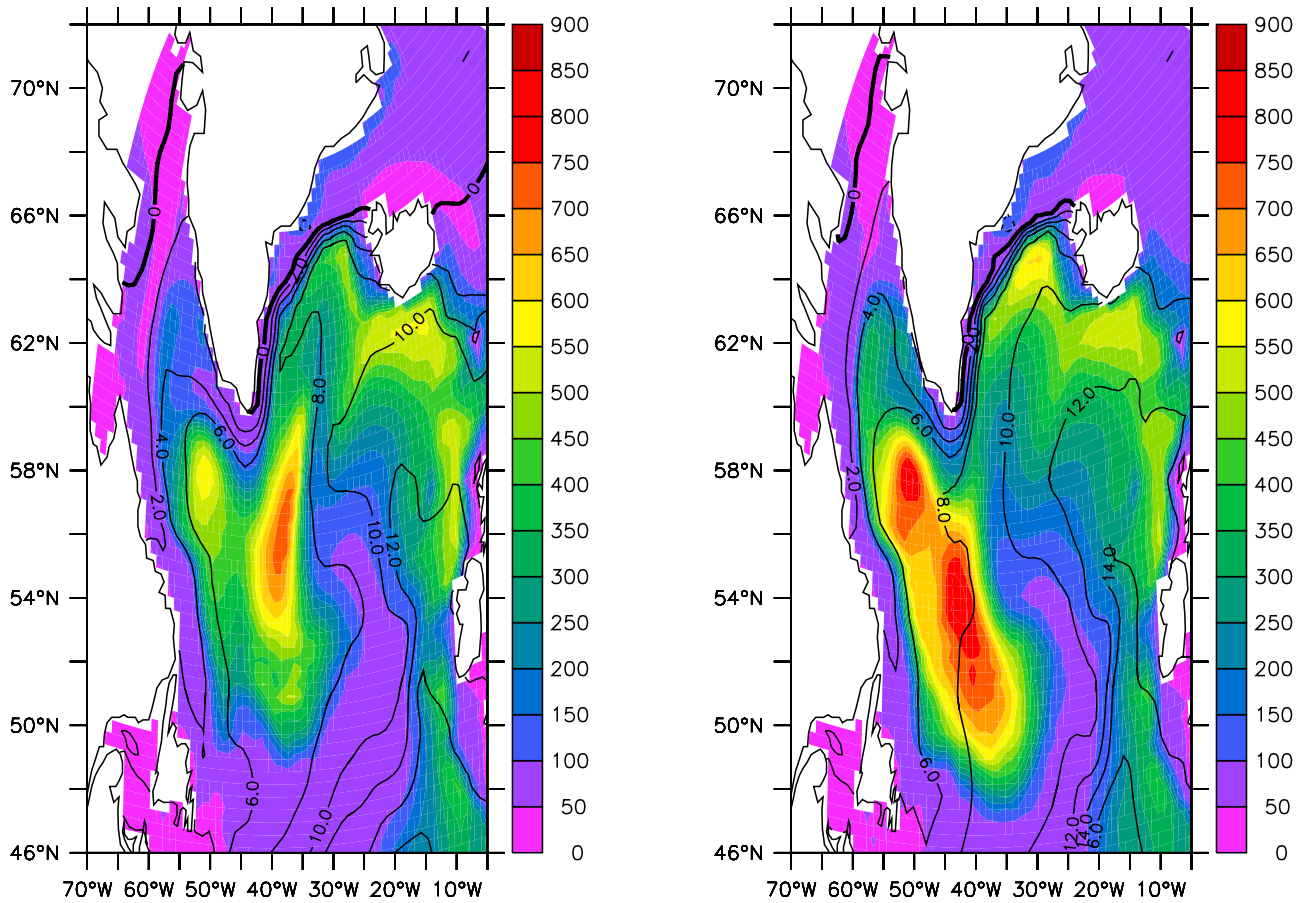
Figure 14. Annual maximum mixed layer depth (color bar) and mean SST (contour interval is 2°C) for (left) CONT and (right) LEPSI. Note the differences in the tongues of warm SST, consistent with the isopycnal differences shown in Figure 13. In the absence of recorded individual convection events, the maximum mixed layer depth is used here as a proxy for convective activity.
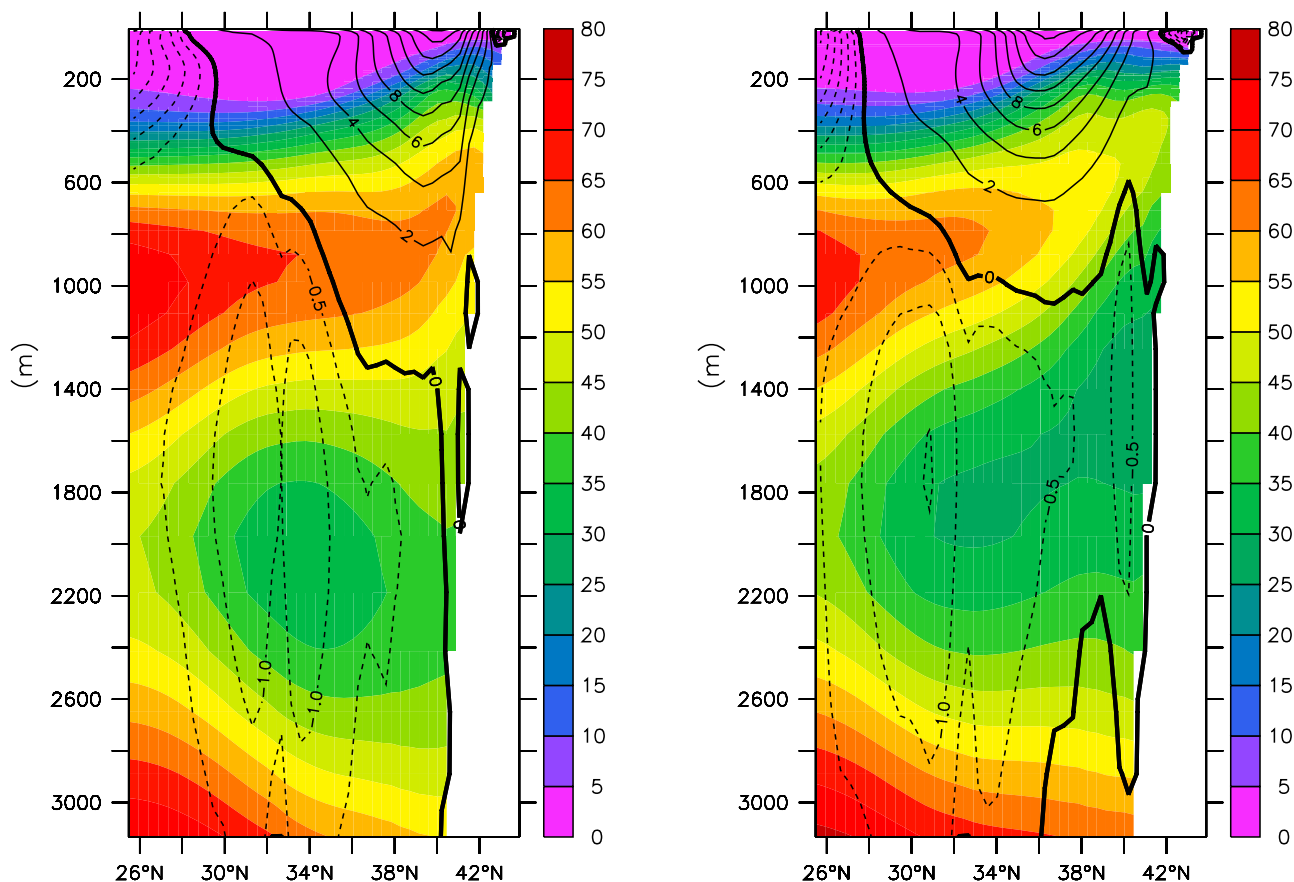
Figure 15. Ideal age (color) and alongshore velocity (contour lines are 2 cm/s for eastward and 0.5 cm/s for westward flow) at 65°W for (left) CONT and (right) LEPSI. Note that in CONT the Gulf Stream (eastward flow) extends all the way to 2000 m depth, and there is no DWBC, only sluggish westward flow in the interior. In LEPSI the Gulf Stream is shifted south, and there is now a DWBC flowing west along the coast. This DWBC now creates a core of relatively young water which spreads along the coast.

separation and the Labrador Sea water properties are worsened, although it is promising that in LEPSI there is now a distinct core of Labrador Sea water flowing south along the North American continent.

[36] Incorporating the observed latitudinal structure is only one step toward a more accurate representation of vertical diffusivities in OGCMs. Previous steps incorporated tidally induced mixing over bottom topography [*Jayne*, 2008] and in the Banda Sea [*Jochum and Potemra*, 2008], and future work will have to include a representation of the increased diffusivities in the Southern Ocean (e.g., *Kunze et al.* [2006], see also the description of the field experiment DIMES: http://dimes.ucsd.edu). From the modeling perspective, though, it appears of critical importance to obtain more observational estimates of equatorial and of North Atlantic thermocline diffusivities.

[37] There is one fundamental question that is avoided here, but has to be addressed in the future: On what level should the breaking of internal waves be incorporated into climate models? Constant diffusivity is certainly the most primitive way, and the present study is only a small step up. For the tidally induced component of vertical mixing, progress has been made with direct modeling of tides and using observations for validation [*Simmons et al.*, 2004;

Koch-Larrouy et al., 2007; *Schiller and Fiedler*, 2007]. Modeling the wind induced part of mixing appears to be more challenging, partly because of the nonlocal structure of the problem, and partly because the relevant scales are still being debated [e.g., *Nagasawa et al.*, 2000; *Zhai et al.*, 2007]. Arguably, for the task of climate prediction the wind induced mixing is more relevant since it could allow for an additional feedback between SST and the strength and variability of atmospheric forcing.

References

Alford, M. H., J. A. MacKinnon, Z. Zhao, R. Pinkel, J. Klymak, and T. Peacock (2007), Internal waves across the Pacific, *Geophys. Res. Lett.*, *34*, L24601, doi:10.1029/2007GL031566.

Bailey, D. A., P. B. Rhines, and S. Haekkinen (2005), Formation and pathways of North Atlantic Deep Water in a coupled ice-ocean model of the Arctic-North Atlantic Oceans, *Clim. Dyn.*, *25*, 497–516.

Bala, G., R. B. Rood, A. Mirin, J. McClean, K. Achutarao, D. Bader, P. Gleckler, R. Neale, and P. Rasch (2008), Evaluation of a CCSM3 simulation with a finite volume dynamical core, *J. Clim.*, *21*, 1467–1485.

Bryan, F. O. (1987), Parameter sensitivity of primitive ocean circulation models, *J. Phys. Oceanogr.*, *17*, 970–985.

Bryan, K., and L. J. Lewis (1979), A water mass model of the world ocean, *J. Geophys. Res.*, *84*, 2503–2516.

Collins, W. D., et al. (2006), The Community Climate System Model: CCSM3, *J. Clim.*, *19*, 2122–2143.

Davis, R. E. (1994a), Diapycnal mixing in the ocean: Equations for large-scale budgets, *J. Phys. Oceanogr.*, *24*, 777–800.

Davis, R. E. (1994b), Diapycnal mixing in the ocean: The Osborn-Cox model, *J. Phys. Oceanogr.*, *24*, 2560–2576.

Ezer, T., and G. L. Mellor (1992), A numerical study of the variability and separation of the Gulf Stream, *J. Phys. Oceanogr.*, *22*, 660–682.

Ffield, A., and A. L. Gordon (1992), Vertical mixing in the Indonesian thermocline, *J. Phys. Oceanogr.*, *22*, 184–195.

Fine, R. (1987), The penetration of tritium into the tropical Pacific, *J. Phys. Oceanogr.*, *17*, 553–564.

Garabato, A. C. N., K. L. Polzin, B. A. King, K. J. Heywood, and M. Visbeck (2004), Widespread intense turbulent mixing in the Southern Ocean, *Science*, *303*, 210–213.

Gent, P., F. O. Bryan, G. Danabasoglu, K. Lindsay, D. Tsumune, M. W. Hecht, and S. C. Doney (2006), Ocean chlorofluorocarbon and heat uptake during the twentieth century in the CCSM3, *J. Clim.*, *19*, 2366–2381.

Gerdes, R., and C. Koeberle (1995), On the influence of the DSOW in a numerical model of the North Atlantic circulation, *J. Phys. Oceanogr.*, *25*, 2624–2641.

Gill, A. (1980), Some simple solutions for heat-induced tropical circulation, *Q. J. R. Meteorol. Soc.*, *106*, 447–462.

Gregg, M. C. (1977), Variations in the intensity of small-scale mixing in the thermocline, *J. Phys. Oceanogr.*, *7*, 436–454.

Gregg, M. C., T. B. Sanford, and D. P. Winkel (2003), Reduced mixing from the breaking of internal waves in equatorial waters, *Nature*, *422*, 513–515.

Griffies, S. M., R. C. Pacanowski, and R. W. Hallberg (2000), Spurious diapycnal mixing associated with advection in a z-coordinate model, *Mon. Wea. Rev.*, *128*, 538–564.

Harper, S. (2000), Thermocline ventilation and pathways of tropical-subtropical water mass exchange, *Tellus*, *52*, 330–345.

Harrison, M. J., and R. Hallberg (2008), Pacific subtropical cell response to reduced equatorial dissipation, *J. Phys. Oceanogr.*, *38*, 1894–1912.

Hibiya, T., and M. Nagasawa (2004), Latitudinal dependence of diapycnal diffusivity in the thermocline estimated using a fine-scale parameterization, *Geophys. Res. Lett.*, *31*, L01301, doi:10.1029/2003GL017998.

Jayne, S. R. (2008), The impact of abyssal mixing parameterizations in an ocean general circulation model, *J. Phys. Oceanogr.*, in press.

Jochum, M., and J. Potemra (2008), Sensitivity of tropical rainfall to Banda Sea diffusivity in the Community Climate System Model, *J. Clim.*, *21*, 6445–6454.

Jochum, M., G. Danabasoglu, M. Holland, Y.-O. Kwon, and W. Large (2008), Ocean viscosity and climate, *J. Geophys. Res.*, *113*, C06017, doi:10.1029/2007JC004515.

Johnson, G. C., M. J. McPhaden, and E. Firing (2001), Equatorial Pacific ocean horizontal velocity, divergence and upwelling, *J. Phys. Oceanogr.*, *31*, 839–849.

Kelley, D. E., and K. A. V. Scoy (1999), A basinwide estimate of vertical mixing in the upper thermocline: spreading of bomb tritium in the North Pacific Ocean, *J. Phys. Oceanogr.*, *29*, 1759–1771.

Koch-Larrouy, A., G. Madec, P. Bouruet-Aubertot, T. Gerkema, L. Bessières, and R. Molcard (2007), On the transformation of Pacific water into Indonesian Throughflow water by internal tidal mixing, *Geophys. Res. Lett.*, *34*, L04604, doi:10.1029/2006GL028405.

Kunze, E., E. Firing, J. M. Hummon, T. K. Chereskin, and A. M. Thurnherr (2006), Global abyssal mixing inferred from lowered ADCP shear and CTD strain profiles, *J. Phys. Oceanogr.*, *36*, 1553–1576.

Large, W. G., and G. Danabasoglu (2006), Attribution and impacts of upper-ocean biases in CCSM3, *J. Clim.*, *19*, 2325–2346.

Large, W. G., and S. Yeager (2008), The global climatology of an inter-annually varying air-sea flux dataset, *Clim. Dyn.*, doi:10.1007/s00382-008-00441-3, in press.

Large, W. G, J. C. McWilliams, and S. C. Doney (1994), Oceanic vertical mixing— A review and a model with nonlocal parameterization, *Rev. Geophy.*, *32*, 363–403.

Ledwell, J. R., A. J. Watson, and C. S. Law (1993), Evidence for slow mixing across the pycnocline from an open ocean tracer release experiment, *Nature*, *364*, 701–703.

Ledwell, J. R., A. J. Watson, and C. S. Law (1998), Mixing of tracer in the pycnocline, *J. Geophys. Res.*, *103*, 21,499–21,529.

Levitus, S., C. Stephens, J. Antonov, and T. P. Boyer (1998), *World Ocean Database 1998, Volume 1: Introduction, NOAA Atlas NESDIS*, vol. 18, 346 pp., U.S. Gov. Print. Off., Washington, D. C.

Liu, Z., and S. Philander (1995), How different wind stress patterns affect the tropical-subtropical circulations of the upper ocean, *J. Phys. Oceanogr.*, *25*, 449–462.

Livezey, R. E., M. Masutani, A. Leetmaa, H. Rui, M. Ji, and A. Kumar (1997), Teleconnective response of the Pacific North American region atmosphere to large central equatorial Pacific SST anomalies, *J. Clim.*, *10*, 1787–1820.

Luyten, J., J. Pedlosky, and H. Stommel (1983), The ventilated thermocline, *J. Phys. Oceanogr.*, *13*, 292–309.

MacKinnon, J. A., and K. B. Winters (2005), Subtropical catastrophe: Significant loss of low-mode tidal energy at $28.9°$, *Geophys. Res. Lett.*, *32*, L15605, doi:10.1029/2005GL023376.

Maes, C., G. Madec, and P. Delecluse (1997), Sensitivity of an equatorial Pacific OGCM to the lateral diffusion, *J. Phys. Oceanogr.*, *125*, 958–971.

McComas, C. H. (1977), Equilibrium mechanisms within the ocean internal wave field, *J. Phys. Oceanogr.*, *7*, 836–845.

McCreary, J., and P. Lu (1994), Interaction between the subtropical and equatorial ocean circulations: The subtropical cell, *J. Phys. Oceanogr.*, *24*, 466–497.

McCreary, J., P. Lu, and Z. Yu (2002), Dynamics of the Pacific subsurface countercurrents, *J. Phys. Oceanogr.*, *32*, 2379–2404.

McWilliams, J. C., G. Danabasoglu, and P. R. Gent (1996), Tracer budgets in the warm water sphere, *Tellus*, *48*, 179–192.

Menemenlis, D., I. Fukumori, and T. Lee (2005), Using Greens functions to calibrate an ocean general circulation model, *Mon. Wea. Rev.*, *133*, 1224–1240.

Moum, J. N., D. R. Caldwell, J. D. Nash, and G. D. Gunderson (2002), Observations of boundary mixing over the continental slope, *J. Phys. Oceanogr.*, *32*, 2113–2129.

Müller, P., G. Holloway, F. Henyey, and N. Pomphrey (1986), Nonlinear interaction among internal gravity waves, *Rev. Geophys.*, *24*, 493–536.

Munk, W. (1966), Abyssal Recipes, *Deep Sea Res.*, *13*, 707–730.

Munk, W., and C. Wunsch (1998), Abyssal recipies II: Energetics of tidal and wind mixing, *Deep Sea Res. I*, *45*, 1977–2010.

Nagasawa, M., Y. Niwa, and T. Hibiya (2000), Spatial and temporal distribution of the wind-induced internal energy available for deep water mixing in the North Pacific, *J. Geophys. Res.*, *105*, 13,933–13,943.

Neale, R., J. Richter, and M. Jochum (2008), From a delayed oscillator to a series of events: Yhe impact of convection parameterization on ENSO, *J. Clim.*, *21*, 5904–5924.

Schiller, A., and R. Fiedler (2007), Explicit tidal forcing in an ocean general circulation model, *Geophys. Res. Lett.*, *34*, L03611, doi:10.1029/2006GL028363.

Schott, F. A., and J. P. McCreary (2001), The monsoon circulation of the Indian Ocean, *Progr. Oceanogr.*, *51*, 1–123.

Scott, J., and J. Marotzke (2002), The location of diapycnal mixing and the meridional overturning circulation, *J. Phys. Oceanogr.*, *32*, 3578–3595.

Simmons, H. L. (2008), Spectral modification and geographical redistribution of the semi-diurnal internal tide, *Ocean Modell.*, *21*, 126–138.

Simmons, H. L., S. R. Jayne, L. C. S. Laurent, and A. J. Weaver (2004), Tidally driven mixing in a numerical model of the ocean general circulation, *Ocean Modell.*, *6*, 245–263.

Speer, K., and E. Tziperman (1992), Rates of watermass formation in the North Atlantic Ocean, *J. Phys. Oceanogr.*, *22*, 93–104.

Sriver, R. L., and M. Huber (2007), Observational evidence for an ocean heat pump induced by tropical cyclones, *Nature*, *447*, 577–580.

Stammer, D. (2005), Adjusting internal model errors through ocean state estimation, *J. Phys. Oceanogr.*, *35*, 1143–1153.

Steele, R. D., R. Morley, and W. Ermold (2001), PHC: A global ocean hydrography with a high quality Arctic Ocean, *J. Clim.*, *14*, 2079–2087.

Thompson, A. F., S. T. Gille, J. A. MacKinnon, and J. Sprintall (2007), Spatial and temporal patterns of small-scale mixing in the Drake Passage, *J. Phys. Oceanogr.*, *37*, 572–592.

Thompson, J. D., and W. J. Schmitz (1989), A limited area model of the Gulf Stream: Design, initial experiments and model data intercomparison, *J. Phys. Oceanogr.*, *19*, 791–814.

Tian, J., L. Zhou, and X. Zhang (2006), Latitudinal distribution of mixing rate caused by the M2 internal tide, *J. Phys. Oceanogr.*, *36*, 35–42.

Trenberth, K. E., G. W. Branstator, D. Karoly, A. Kumar, N.-C. Lau, and C. Ropelewski (1998), Progress during TOGA in understanding and modeling global teleconnections associated with tropical SST, *J. Geophys. Res.*, *103*, 14,291–14,324.

Walin, G. (1982), On the relation between the sea surface heat flow and thermal circulation in the ocean, *Tellus*, *34*, 187–195.

Warren, B. A. (1981), Deep circulation of the world ocean, in *Evolution in Physical Oceanography: Scientific Surveys in Honor of Henry Stommel*, edited by B. A. Warren and C. Wunsch, pp. 6–41, Mass. Inst. of Technol. Press, Cambridge, Mass.

Weaver, J., and E. Sarachik (1990), On the importance of vertical resolution in certain ocean general circulation models, *J. Phys. Oceanogr.*, *20*, 600–609.

Wunsch, C., and R. Ferrari (2004), Vertical mixing, energy and the general circulation of the oceans, *Annu. Rev. Fluid Mech.*, *36*, 281–314.

Wüst, G. (1949), Über die zweiteilung der hydrosphäre, *Dtsch. Hydrogr. Z.*, *2*, 218–225.

Zhai, X., R. J. Greatbatch, and C. Eden (2007), Spreading of near-inertial energy in a 1/12° model of the North Atlantic Ocean, *Geophys. Res. Lett.*, *34*, L10609, doi:10.1029/2007GL029895.

Zhang, R., and G. K. Vallis (2007), The role of bottom vortex stretching on the path of the North Atlantic western boundary current and on the northern recirculation gyre, *J. Phys. Oceanogr.*, *37*, 2053–2077.

————————————

M. Jochum, National Center for Atmospheric Research, 1850 Table Mesa Drive, Boulder, CO 80305, USA. (markus@ucar.edu)